

On the Low-Latitude Ionospheric Irregularities under Geomagnetically Active and Quiet Conditions using NavIC observables: A Spectral Analysis Approach

Sumanjit Chakraborty^{a,b,*}, Abhirup Datta^a

^a*Department of Astronomy, Astrophysics and Space Engineering, Indian Institute of Technology Indore, Simrol, Indore 453552, Madhya Pradesh, India*

^b*Indian Institute of Geomagnetism, Navi Mumbai, India*

Abstract

Ionospheric irregularities and associated scintillations under geomagnetically active/quiet conditions have detrimental effects on the reliability and performance of space- and ground-based navigation satellite systems, especially over the low-latitude region. The current work investigates the low-latitude ionospheric irregularities using the phase screen theory and the corresponding temporal Power Spectral Density (PSD) analysis to present an estimate of the outer irregularity scale sizes over these locations. The study uses simultaneous L5 signal C/N_0 observations of NavIC (a set of GEO and GSO navigation satellite systems) near the northern crest of EIA (Indore: 22.52°N, 75.92°E, dip: 32.23°N) and in between the crest and the dip equator (Hyderabad: 17.42°N, 78.55°E, dip: 21.69°N). The study period (2017-2018) covers disturbed and quiet-time conditions in the declining phase of the solar cycle 24. The PSD analysis brings forward the presence of irregu-

*Corresponding author.

Email addresses: sumanjit11@gmail.com (Sumanjit Chakraborty), abhirup.datta@iiti.ac.in (Abhirup Datta)

larities, of the order of a few hundred meters during weak-to-moderate and quiet-time conditions and up to a few km during the strong event, over both locations. The ROTI values validate the presence of such structures in the Indian region. Furthermore, only for the strong event, a time delay of scintillation occurrence over Indore, with values of 36 minutes and 50 minutes for NavIC satellites (PRNs) 5 and 6, respectively, from scintillation occurrence at Hyderabad is observed, suggesting a poleward evolution of irregularity structures. Further observations show a westward propagation of these structures on this day. This study brings forward the advantage of utilizing continuous data from the GEO and GSO satellite systems in understanding the evolution and propagation of the ionospheric irregularities over the low-latitude region.

Keywords:

Ionospheric Scintillation, Ionospheric Irregularities, NavIC, Power Spectral Density, ROTI

1. Introduction

The phenomenon of scintillation can be thought of as analog to the stars that twinkle in the night sky as a result of variations in the density of the atmosphere due to turbulence. The phenomenon of plasma instability (post-sunset) in the equatorial ionosphere generates irregularities and large-scale depletions in the electron density referred to as the Equatorial Plasma Bubbles (EPBs) (Yeh and Liu (1982) and references therein). Radio waves propagating through these irregularities experience diffraction and scattering, which cause random fluctuations in the VHF and L-band signal

amplitude, phase, the direction of propagation, and polarization referred to as scintillations (Carrano et al., 2011, 2012a; Priyadarshi, 2015). It is well known that the irregularities that produce scintillations are mainly found in the F layer of the ionosphere (~ 300 - 350 km), where the plasma density has the maximum value. Rayleigh–Taylor (R-T) instabilities are considered as the primary mechanism generating EPBs with scale sizes from a few hundred meters to several kilometers (Priyadarshi, 2015). Activities of scintillations are generally observed during the period of maximum solar activity, occurring near the magnetic equator in the post-sunset-to-midnight sector (Basu et al., 1988a,b). It is well known that ionospheric scintillations are demonstrations of space weather effects, affecting the performance of space-based navigation and communication systems that rely on transionospheric radio-wave propagation (Carrano et al., 2012a; de Oliveira Moraes et al., 2017).

For characterizing radio wave scintillation that travels in the ionosphere, numerous phase screen theories have been developed, as early as the 1950s following works done by (Booker et al., 1950; Hewish and Bragg, 1951). Generally, the scintillation of radio waves is calculated using the theory of wave propagation in random media to obtain the parameters of the exiting wave from the ionosphere. It is performed by solving the Fresnel diffraction theory problem involving the propagation of these waves traveling between the ionosphere and the Earth. Thus, these calculations replace the ionosphere with an equivalent phase screen that is random, where the irregularities in the ionosphere are considered as phase objects (Taylor and Infosino, 1976). Simultaneously, the ground pattern produced by radio waves propagating through this screen is derived from the diffraction theory (Bhattacharyya,

1999). In general, the one- and two-dimensional phase screens are analytic representations of the intensity of the spectral density function in terms of the various phase structure function combinations (Carrano and Rino, 2016). Phase screen models have been extensively used to simulate the distortion of wideband waveforms for communications (Knepp and Nickisch, 2009), fading of GNSS satellite signals, and scintillation of satellite signals used in radio occultation experiments, to name a few. These phase screen models' inputs are the in-situ electron density measurements, a radio receiver's time series phase measurements, and a turbulent ionospheric medium-based stochastic model.

Several researchers (Carrano et al. (2011, 2012a); de Oliveira Moraes et al. (2017); Aol et al. (2020); Liu et al. (2012) and references therein) have addressed in-situ electron density fluctuations measured by the satellites to predict the propagation effects. However, the disadvantage lies in the fact that measured values sample the electron density irregularities and fluctuations at the satellite's orbital altitude. The transionospheric propagation effects can be attributed to the integrated development of the density variation along the signal ray path at all altitudes. If any, the relation between density fluctuations sampled at one altitude to another is still not evident in the literature. Therefore, if the density irregularities associated with an EPB have not risen to the satellite's altitude that measures the in-situ density values, detection of fluctuations will be absent despite the EPB causing radio scintillations as a result of the irregularities present at lower altitudes. There is an advantage of probing the ionosphere at all altitudes, from the ground-based observations of signal phase transmitted by a satellite at the topside ionosphere or

beyond, over in-situ electron density observations. Thus, it becomes essential to understand and quantify the contribution from phase scintillations caused by diffraction, in addition to interpreting the signal phase time series and the corresponding limitations of judiciously representing the structure of irregularity at these altitudes (Secan et al., 1995; Carrano et al., 2012a; Bhattacharyya et al., 2000; Knepp, 2004; Caton et al., 2009; Costa et al., 2011).

The presence of the northern crest of the Equatorial Ionization Anomaly (EIA) and the geomagnetic equator that touches the southern tip of the Indian peninsular region, accompanied by sharp latitudinal gradients of ionization, make the Indian longitude sector a highly geosensitive region of investigation for ionospheric research during geomagnetically disturbed periods when the low-latitude ionization is significantly affected as a result of solar eruptions like the Coronal Mass Ejections (CMEs) (Chakraborty et al., 2020; Chakraborty and Datta, 2020b; Chakraborty and Datta, 2020c; Chakraborty, 2022; Chakraborty and Chakrabarty, 2023), the coronal hole-high speed solar wind streams associated co-rotating interaction regions (Chakraborty et al., 2020a). Although previous studies show the development of power law phase screen theories and models for scintillation using the GPS/GNSS, the nature of ionospheric irregularities using the Navigation with Indian Constellation (NavIC) in the low-latitude region of India, during geomagnetically active as well as quiet-time conditions, has not been studied in the literature. The novelty of this work lies in the simultaneous investigation of the evolution and propagation of low-latitude ionospheric irregularities, during the strong event, over a location (Indore) near the northern crest of the EIA and a

location (Hyderabad) in between the crest and the magnetic equator in Indian sector, utilizing the carrier-to-noise C/N_o observations from a set of geostationary (GEO) and geosynchronous (GSO) satellite system of NavIC.

The manuscript is presented as follows: Section 2 briefly describes the dataset used. Section 3 shows the results and the PSD analysis of the three cases of strong, moderate, and weak event days. Section 4 presents a discussion of these results, while Section 5 presents the summary.

2. Data

The NavIC is a regional navigation satellite system developed by the Indian Space Research Organisation (ISRO). The space segment of NavIC consists of a combination of seven GEO and GSO satellites. It provides continuous (spatial and temporal) monitoring of the upper atmosphere over the low-latitude and equatorial regions in the Indian longitude sector. It is conceived to provide accurate positioning information to all users in and around the 1500 km radius of the boundaries of the country. The suitability of using NavIC for studying the upper atmosphere, over the Indian subcontinent in total and near the EIA (Indore) in particular, has been well established by (Ayyagari et al., 2019; Chakraborty et al., 2020b; Ayyagari et al., 2020; Ayyagari et al., 2020; Chakraborty and Datta, 2020a, 2021; Ayyagari et al., 2021, 2022).

A NavIC receiver is operational at the Department of Astronomy, Astrophysics and Space Engineering of the Indian Institute of Technology Indore (22.52°N, 75.92°E geographic; magnetic dip 32.23°N) since April 2017. It is capable of receiving L5 (1176.45 MHz) and S1 (2492.028 MHz) signals along

with GPS L1 (1575.42 MHz) signals. The output of the receiver includes the carrier-to-noise C/N_o (dB-Hz), azimuth (deg), elevation (deg), pseudo-range (in m), and carrier cycles (cycles). The receiver is provided by the Space Applications Centre, ISRO. Additionally, data from another NavIC receiver operational at the Department of Electronics and Communication Engineering (ECE), Osmania University (OU), Hyderabad (17.42°N, 78.55°E geographic; magnetic dip 21.69°N), has been used. A similar procedure as shown by (Ayyagari et al., 2020) has been followed here for the analysis of these NavIC data. Figure 1 shows the map that contains the locations of observations and the northern crest of the EIA that passes over the Indian sector.

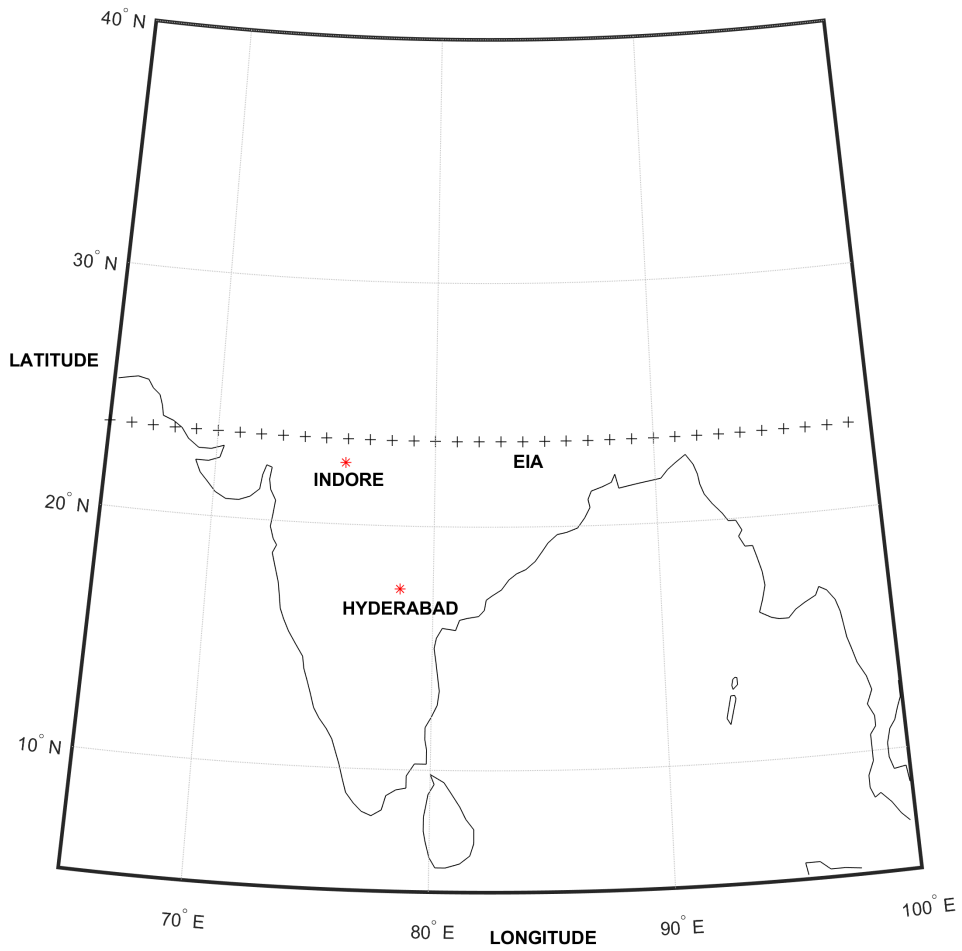


Figure 1: The map of India showing the locations of the two stations and the EIA crest.

3. Results

In this section, the strong storm day of September 08, 2017, the moderate storm day of September 16, 2017, and the weak/minor storm day of August 17, 2018, are presented as sample cases from the 27 days of observations of scintillations during one year, to study the C/N_o variation as observed by the NavIC satellites. The geomagnetic storm intensity in this study is classified following (Loewe and Prolss, 1997). The analyses of the corresponding PSDs are then performed and calculations of the spectral slope and estimation of the outer scale sizes of irregularities, over Indore and Hyderabad, are presented. It is to be noted that as NavIC satellites are at geostationary altitudes, the C/N_o data can be continuously observed throughout the day.

3.1. September 08, 2017: a strong storm day

Due to a CME that arrived on September 06, 2017, a G4 ($K_p=8$, severe) level geomagnetic storm was observed at 23:50 UT on September 07, 2017, at 01:51 UT and 13:04 UT on September 08, 2017, according to the NOAA (<https://www.swpc.noaa.gov/>). Figure 2 shows the interplanetary and geomagnetic conditions on September 08, 2017. The geomagnetic storm had been strong and had a double-peak, evident from Figure 2 (d) showing drops in the SYM-H (nT) values to -146 nT at 01:08 UT and -112 nT at 17:07 UT on the day. The corresponding IMF B_z (nT) in Figure 2 (a) showed values of -20.69 nT and -6.12 nT respectively, suggesting strong southward IMF conditions favorable for an intense geomagnetic storm. The solar wind flow speed, (V_{sw} , km/s), the solar wind density (ρ_{sw} , n/cc), and the K_p values in Figure panels 2 (b), (c), and (e) respectively showed values of 694.3 km/s,

2.91 n/cc and 8 at 01:08 UT and 718 km/s, 3.14 and 7+ at 17:07 UT on
September 08, 2017.

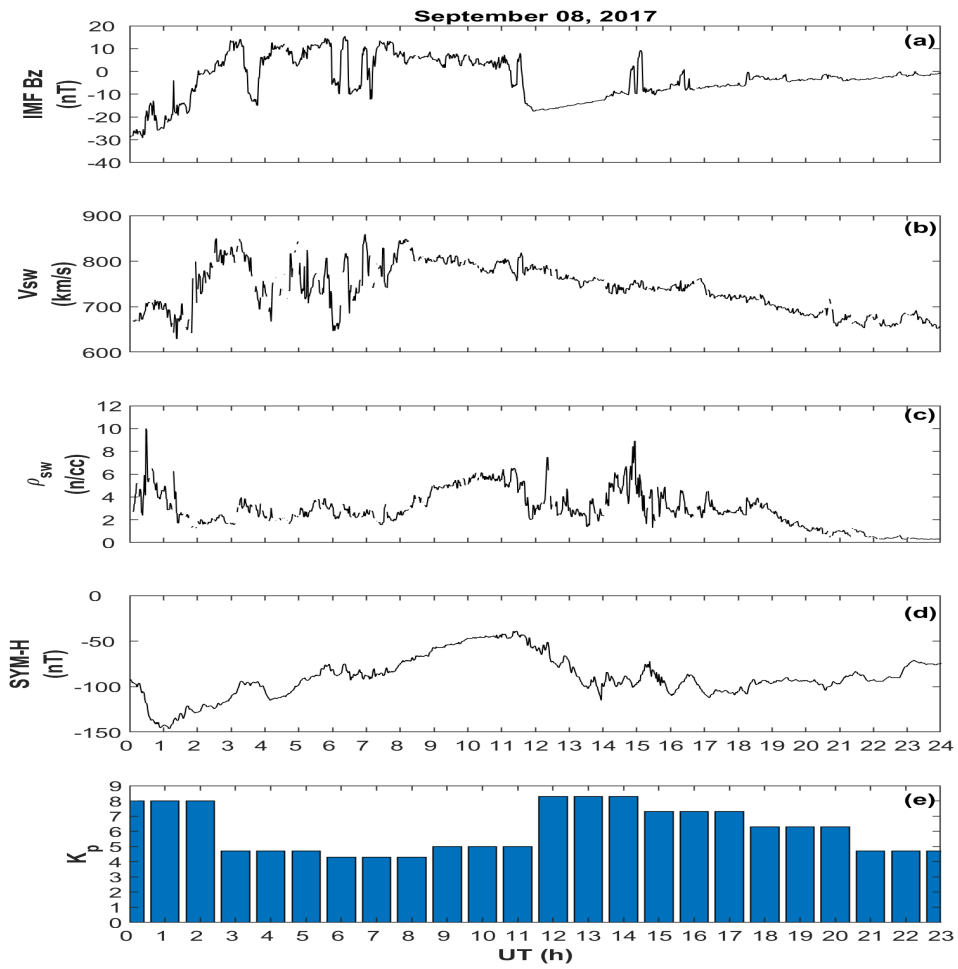


Figure 2: Variations of (a) IMF B_z (nT), (b) V_{sw} (km/s), (c) ρ_{sw} (n/cc), (d) SYM-H (nT) and (e) K_p during September 08, 2017.

Figure 3 shows the C/N_o variation (dB-Hz) over Indore located near the northern crest of the EIA that passes over the highly geosensitive Indian longitude sector, for the entire day of September 08, 2017, as observed by a set of geostationary (PRNs 3, 6 and 7) and geosynchronous (PRNs 2, 4 and 5) satellites of NavIC. The observations are taken by utilizing the L5 (1176.45 MHz) signal of NavIC. Upon closely observing panels showing PRNs 5 and 6 of Figure 3, it is visible that there had been strong fluctuations in the C/N_o with values dropping from about 47 dB-Hz to 36 dB-Hz around 18-19 UT (23:04-00:04(+1) LT) for PRN 5 and from about 51 dB-Hz to 35 dB-Hz around 17-18 UT (22:04-23:04 LT) for PRN 6, which are in between the local pre-midnight and post-midnight sector. It is to be noted that the high value observed in the 14-15 UT bin for PRN5 has not been considered as it is getting manifested as a result of the C/N_o drop to zero observed by this PRN.

To verify whether the observed C/N_o drops in Figure 3 are due to the scintillations that had occurred during this period, Figure 4 shows the hourly binned variance plots of all the PRNs of NavIC during the entire day of September 08, 2017. In bin 18-19 UT for PRN 5 and bin 17-18 UT for PRN 6, the variance over the average values is observed to be significant.

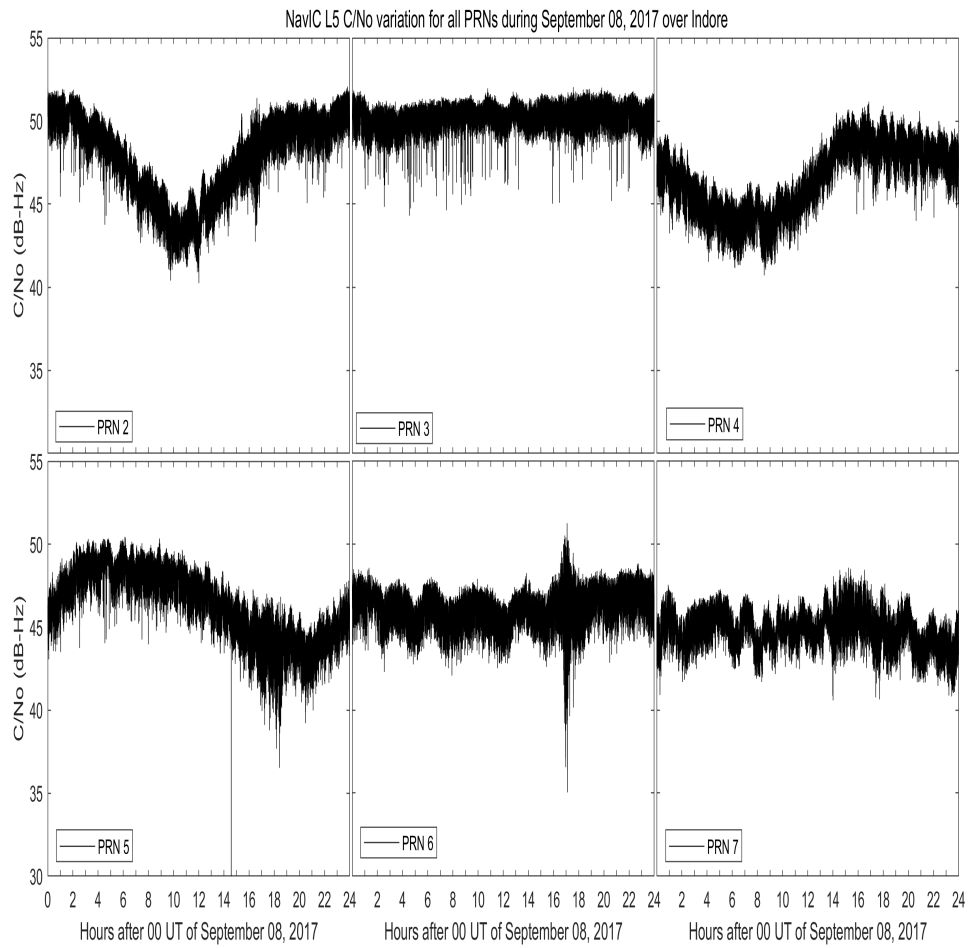


Figure 3: The C/N_o (dB-Hz) variation during the disturbed day of September 08, 2017, as observed by the L5 signal of NavIC satellite PRNs 2-7 over Indore. It is to be noted that the LT = UT + 05:04 h.

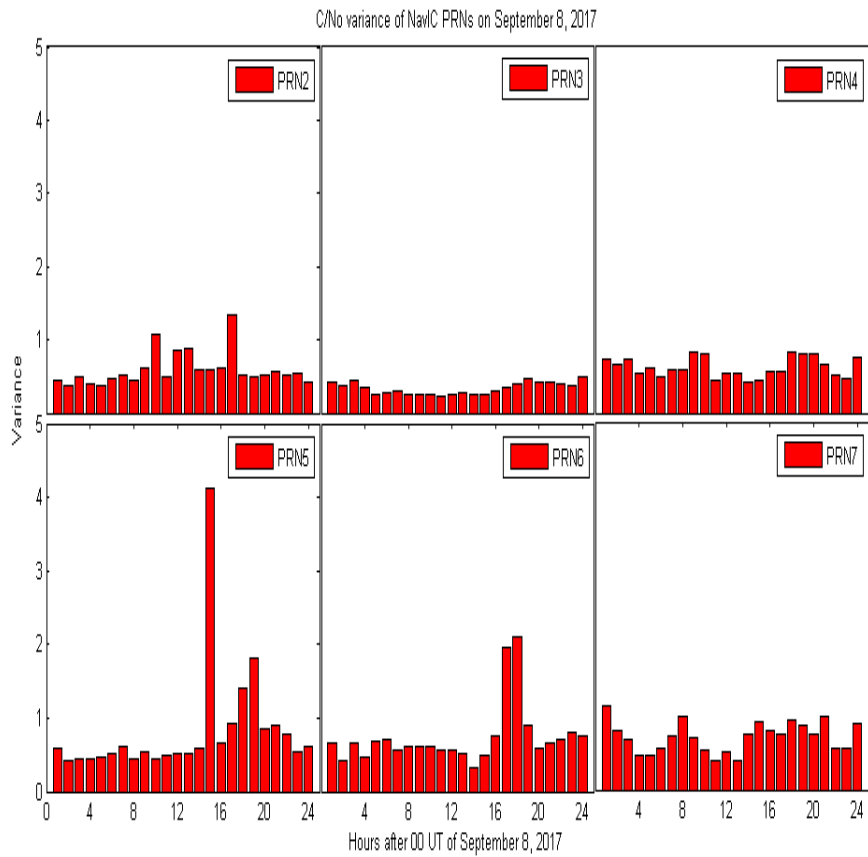


Figure 4: The hourly binned variance plots of C/N_0 for all PRNs of NavIC on September 08, 2017, as observed from Indore. It is to be noted that the $LT = UT + 05:04$ h.

The theory of temporal power spectrum has been introduced by several researchers (Strangeways, 2009; Rino, 1979a,b; Fougere, 1985) as follows:

$$S = \frac{T}{(f_0^2 + f^2)^{\frac{p}{2}}} \quad (1)$$

where f_0 is the outer scale frequency, T is the spectral strength and p is the spectral slope. Equation 1 can be simplified to the following (when $f \gg f_0$):

$$S = T f^{-p} \quad (2)$$

Furthermore, the spectrum of electron density fluctuations (δN) can be modeled as a power law, with an outer scale, given by (Rino, 1979a,b; Carrano et al., 2012b):

$$S_{\delta N}(q) = \frac{C_s}{(q_0^2 + q^2)^{(m+\frac{1}{2})}} \quad (3)$$

where, C_s is the strength of the turbulence proportional to T (Rino, 1979a,b; Carrano et al., 2012b), m is the irregularity spectral index ($p = 2m+1$) and q_0 is the wave number of the outer scale and is related to the outer scale turbulence (L) as:

$$L = \frac{2\pi}{q_0} \quad (4)$$

Therefore, for $q \gg q_0$, the spectrum in equation 3 modifies to:

$$S_{\delta N}(q) = C_s q^{-(2m+1)} = C_s q^{-p} \quad (5)$$

Figure 5 shows the PSD variation from PRN5 and PRN6. The significant time bins (18-19 UT and 17-18 UT for PRNs 5 and 6 respectively) are used for obtaining the PSD variations in this figure. The absolute values of p for the PRNs 5 and 6 are 3.690 ± 0.009 and 3.596 ± 0.008 respectively. These values are obtained from the covariance matrix of the least squares fit

performed to the PSD in the logarithmic domain by using equation 2. These values are then verified with the approximate estimation (Rino, 1979a,b) of $p = \frac{[P(0.05)-P(0.5)]}{10}$ from Figure 5. Further, utilizing equation 5 followed by equation 4, in addition to these spectral slope values from the PSD analysis from equation 2, the outer scale of the irregularities is obtained to be 5.12 ± 0.011 km.

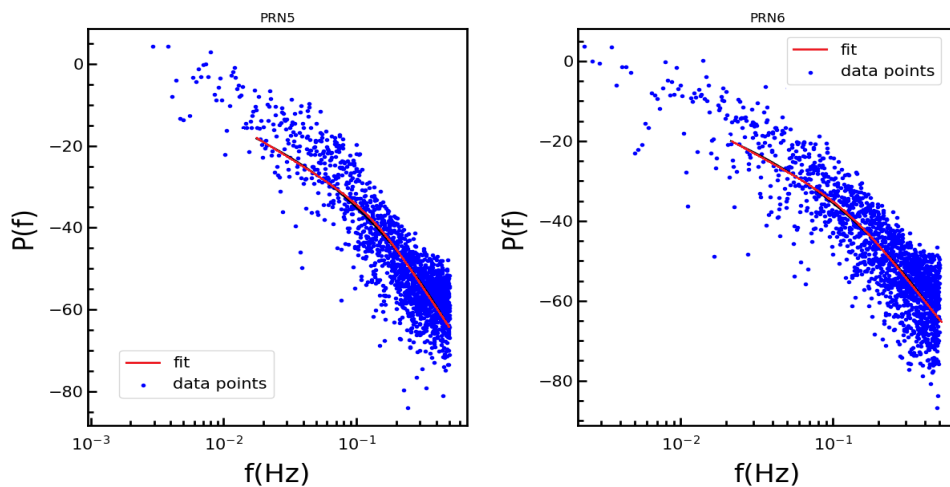


Figure 5: The PSD variations with the least square fit (red solid line) corresponding to the bins of intense C/N_o variation of Figure 4.

Taking a similar approach for the storm day of September 08, 2017, the following Figure 6 shows the NavIC measured C/N_o variation (dB-Hz) over Hyderabad. Upon closely observing panels showing PRNs 5 and 6, it is visible that there had been strong fluctuations in the C/N_o with values dropping from about 50 dB-Hz to 36 dB-Hz around 17-18 UT (22:14-23:14 LT) for PRN 5 and from about 50 dB-Hz to 37 dB-Hz around 16-17 UT (21:14-22:14 LT), both during the local pre-midnight sector.

Similarly, for verification of the observed C/N_o drops due to scintillation,

Figure 7 shows the hourly binned variance plot for all the PRNs of NavIC during the entire day of September 08, 2017. The variance over the average values is significant in the hourly bin of 17-18 UT for PRN 5 and 16-17 UT for PRN 6. Figure 8 shows the PSD variation from the PRNs 5 and 6. The corresponding values of p , using the above equations, for PRNs 5 and 6 are 3.072 ± 0.011 and 3.008 ± 0.010 respectively. The corresponding outer scale size of irregularities obtained is 5.15 ± 0.001 km.

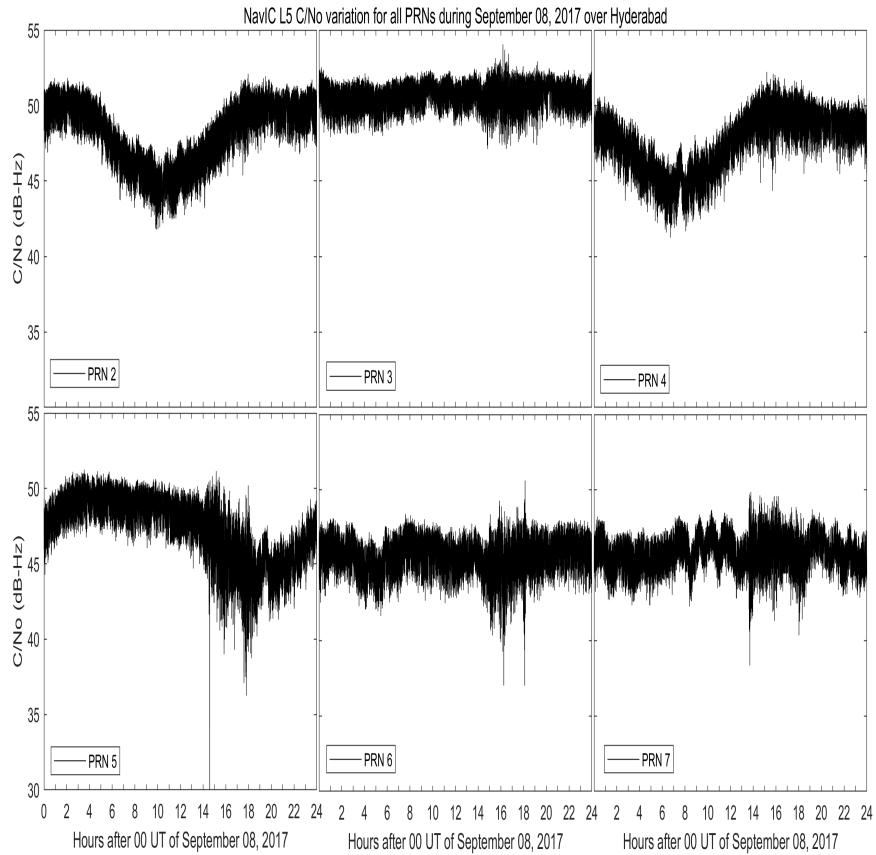


Figure 6: The C/N_o (dB-Hz) variation during the disturbed day of September 08, 2017, as observed by the L5 signal of NavIC satellite PRNs 2-7 over Hyderabad. It is to be noted that the $LT = UT + 05:14$ h.

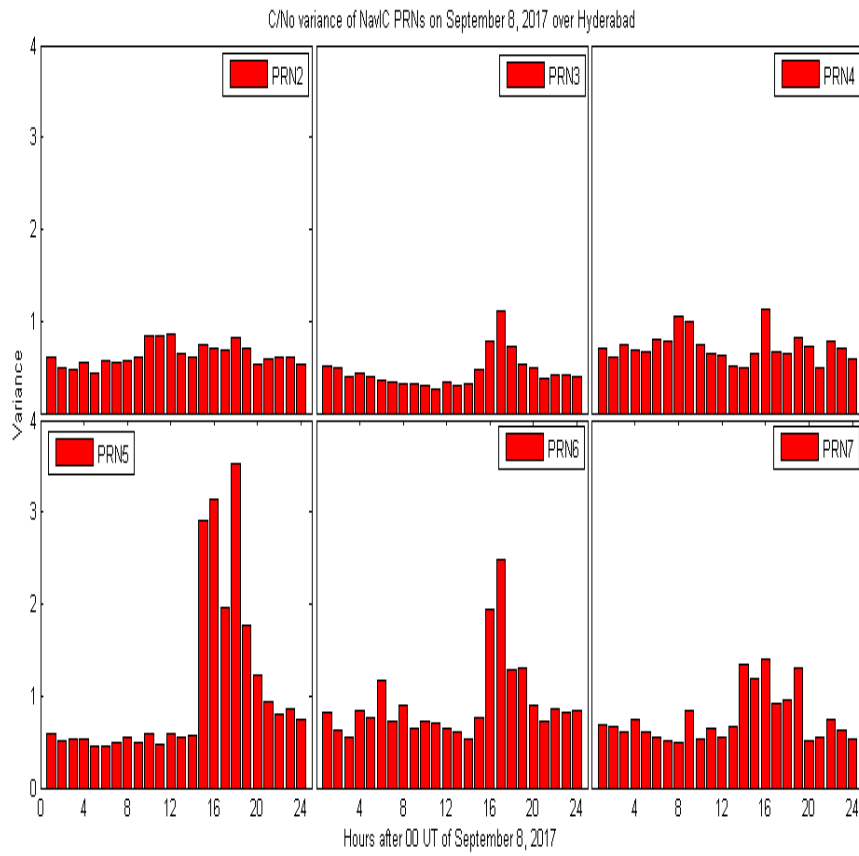


Figure 7: The hourly binned variance plots of C/N_o for all PRNs of NavIC on September 08, 2017, over Hyderabad. It is to be noted that the $LT = UT + 05:14$ h.

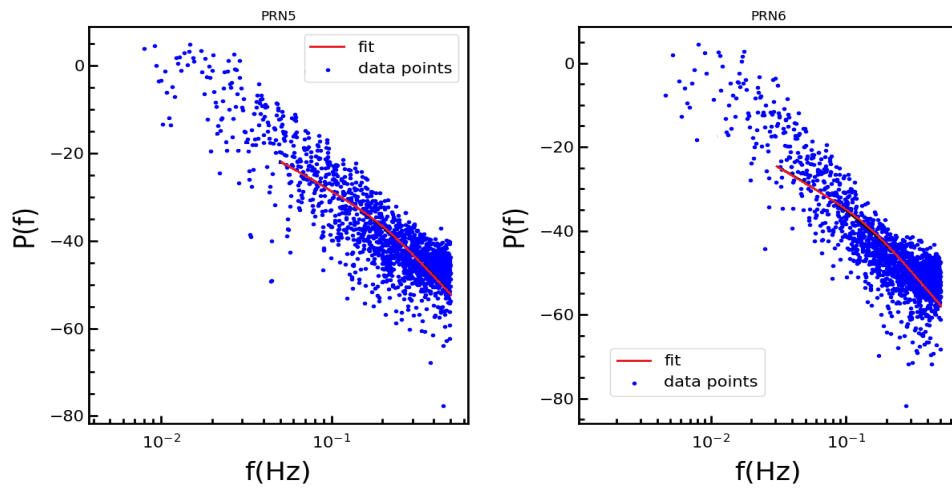


Figure 8: The PSD variations with the least square fit (red solid line) correspond to the time bins of intense C/N_o variation of Figure 7.

3.2. September 16, 2017: a moderate storm day

The high-speed solar wind blew past Earth at a velocity of around 650-850 km/s. This sparked a G2-class (NOAA Space Weather Scales) moderate geomagnetic storm on September 16, 2017. Figure 9 shows the interplanetary and geomagnetic conditions on September 16, 2017. Corresponding to the SYM-H drop (Figure 9 (d)), the IMF B_z , the V_{sw} , the ρ_{sw} , and the K_p values in Figure panels 9 (a), (b), (c), and (e) showed the values of -2.59 nT, 694.3 km/s, 3.56 n/cc and 5+ respectively on September 16, 2017.

Following a similar approach as presented for the previous case, the following Figure 10 shows the C/N_o variation (dB-Hz) for the entire day of September 16, 2017, as observed by the L5 signal of NavIC. Drops in the C/N_o have been observed at multiple time stamps throughout the day by all the PRNs.

However, to confirm whether the C/N_o drops had been significant, Figure 11 has been plotted that shows the hourly binned variance plots of all the PRNs of NavIC during the entire day of September 16, 2017. The hourly bin of 6-7 UT for all the PRNs shows the most significant rise and hence maximum variation among all the bins of the day.

Figure 12 shows the PSD variation from all the satellites of NavIC. It is to be noted that only PRNs 3, 4, and 5 show a power law variation in the PSD and hence are taken into consideration. The values of p for PRNs 3, 4, and 5 are 2.873 ± 0.009 , 2.949 ± 0.009 , and 2.829 ± 0.008 respectively. The corresponding outer irregularity scale size is 0.507 ± 0.001 km.

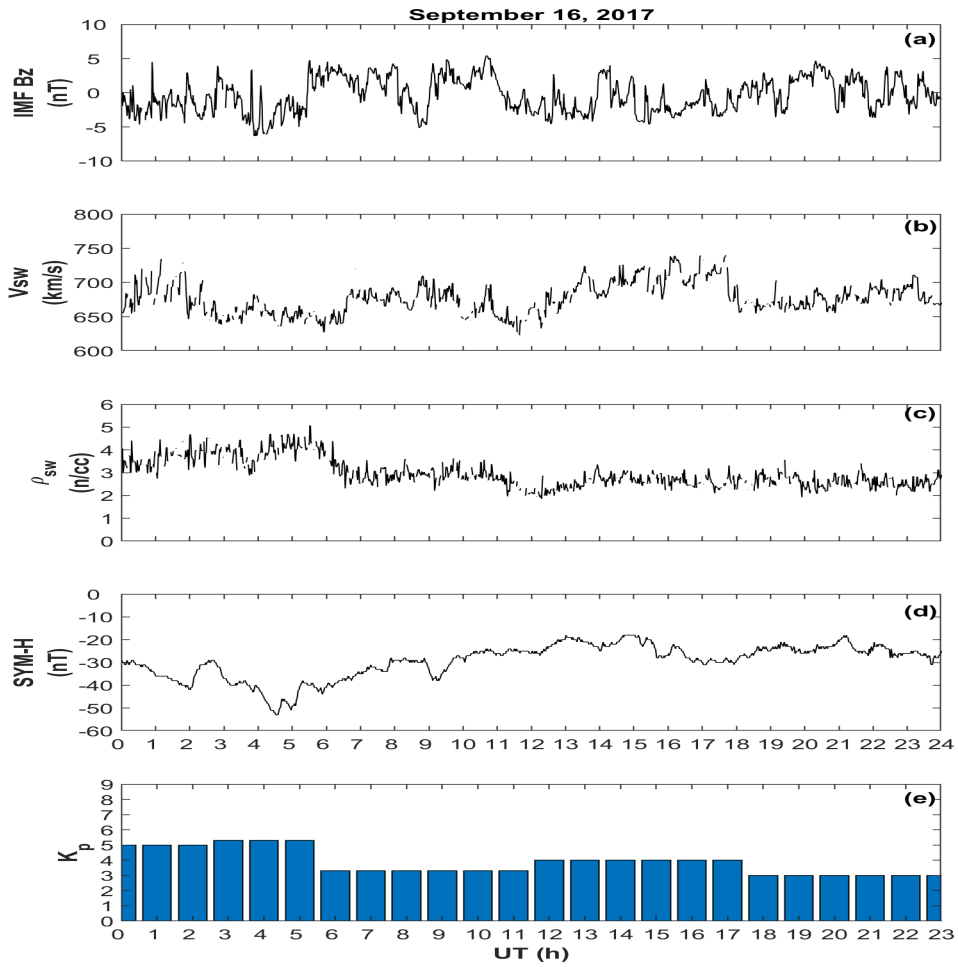


Figure 9: Variations of (a) IMF B_z (nT), (b) V_{sw} (km/s), (c) ρ_{sw} (n/cc), (d) SYM-H (nT) and (e) K_p during September 16, 2017.

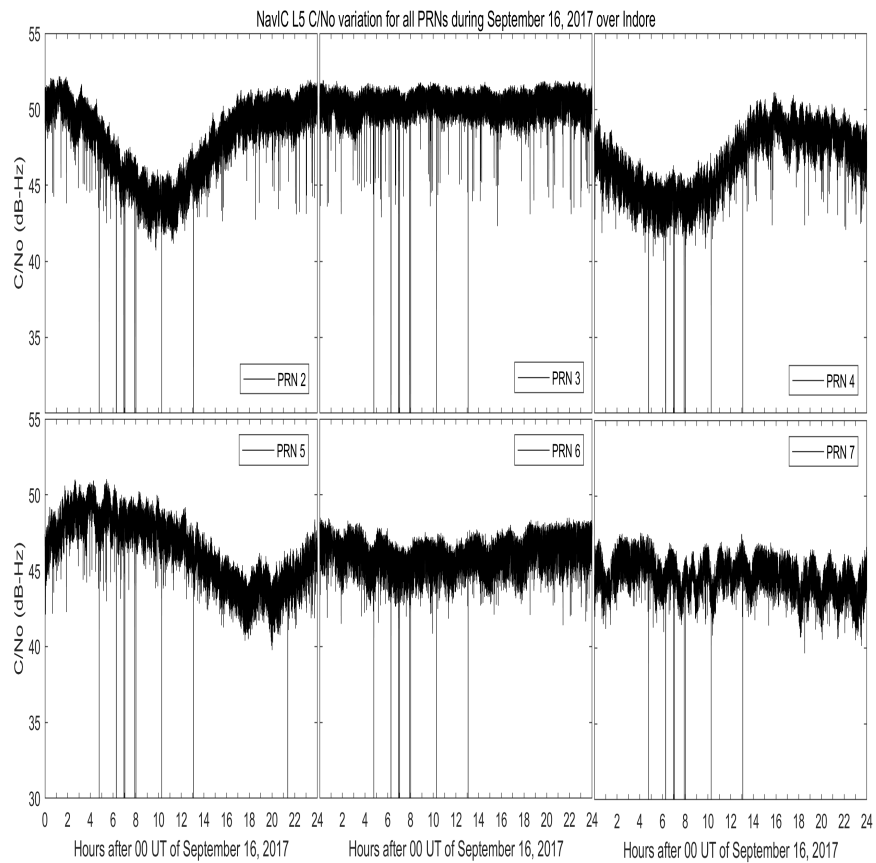


Figure 10: The C/N_o (dB-Hz) variation during the entire day of September 16, 2017, over Indore, as observed by the L5 signal of NavIC satellite PRNs 2-7.

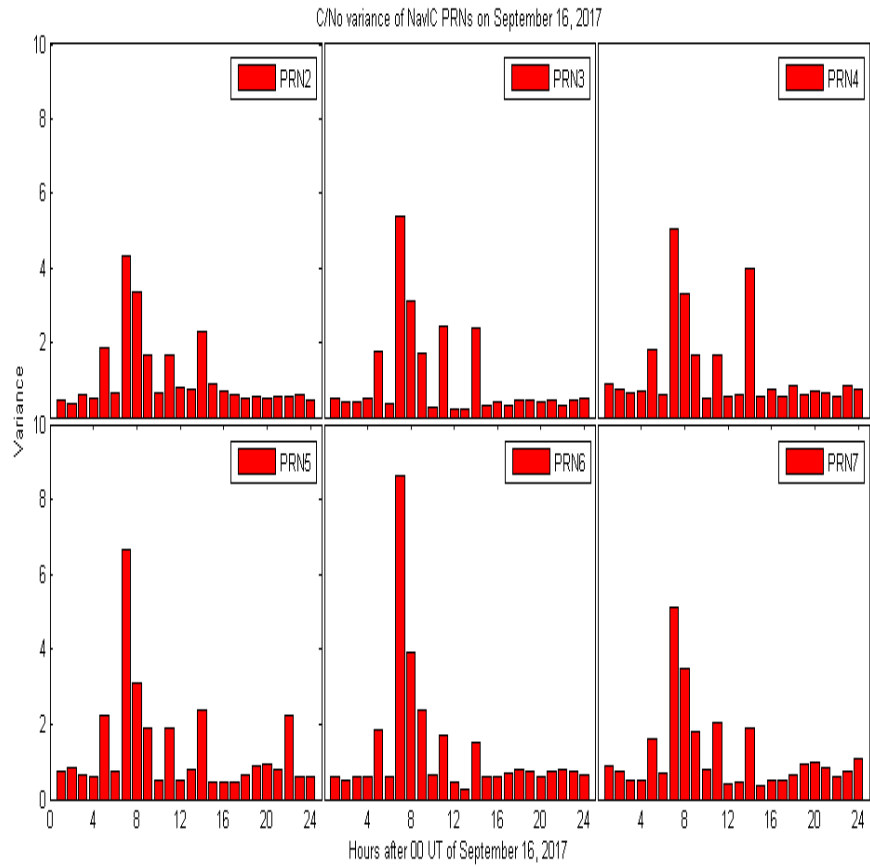


Figure 11: The hourly binned variance plots of C/N₀ for all PRNs of NavIC on September 16, 2017, over Indore.

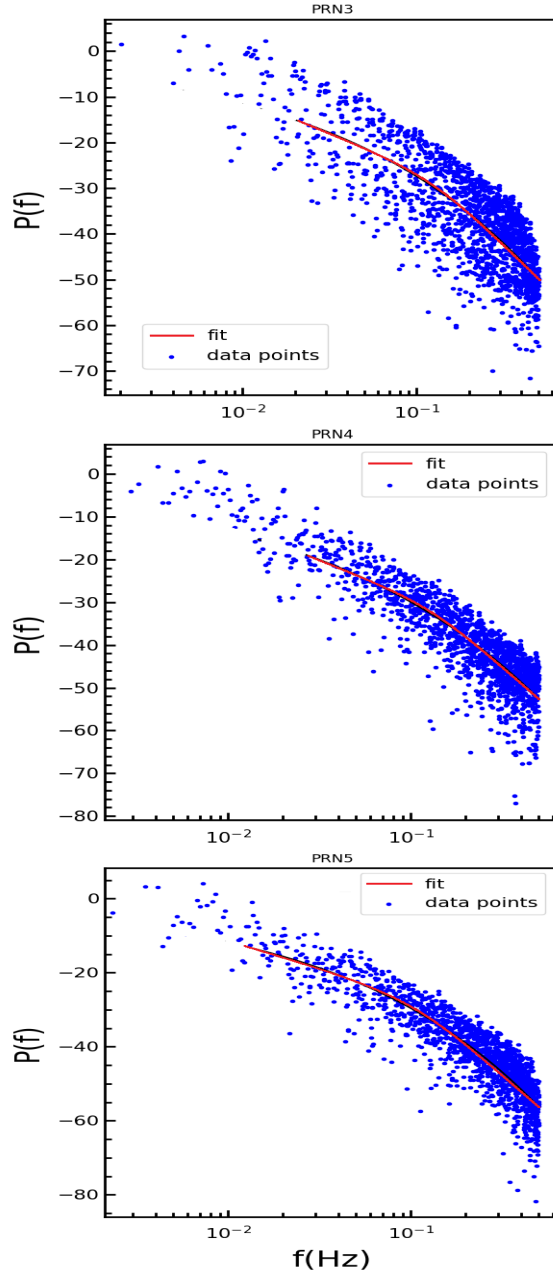


Figure 12: The PSD variations with the least square fit (red solid line) correspond to the time bins of C/N_o variation of Figure 11.

3.3. August 17, 2018: a weak/minor storm day

A solar wind stream hit the geomagnetic field during the late hours of August 15, 2018, and blew throughout the next day. This sparked a G1-class (NOAA Space Weather Scales) weak/minor geomagnetic storm on August 17, 2018. Figure 13 shows the interplanetary and geomagnetic conditions on August 17, 2018. The corresponding values of IMF B_z , the V_{sw} , the ρ_{sw} , and the K_p (shown in Figure panels 13 (a), (b), (c), and (e) respectively), for the SYM-H drops (Figure 13 (d)) are 3.36 nT, 463.5 km/s, 7.50 n/cc, 4 and -2.78 nT, 525.4 km/s, 2.91 n/cc, 3+ respectively on August 17, 2018.

Very similar to the other two cases, Figure 14 shows the C/N_o variation (dB-Hz) for the entire day of August 17, 2018, as observed by the L5 signal of NavIC. Drops in the C/N_o have been observed at multiple time stamps throughout the day by all the PRNs.

However, for the verification of the significance of these C/N_o drops, Figure 15 shows the hourly binned variance plots of all the PRNs of NavIC during the entire day of August 17, 2018. The time bin of 21-22 UT for all the PRNs shows the most significant rise and hence maximum variation among all the bins of this day.

Figure 16, in a way similar to the previous cases, shows the PSD variation from all the NavIC satellites. Here, only PRNs 3, 4, and 6 show the power law variation and hence are taken into consideration. The values of p for PRNs 3, 4, and 6 are 2.306 ± 0.009 , 2.518 ± 0.011 , and 2.322 ± 0.008 respectively. The corresponding outer irregularity scale size is 0.502 ± 0.071 km.

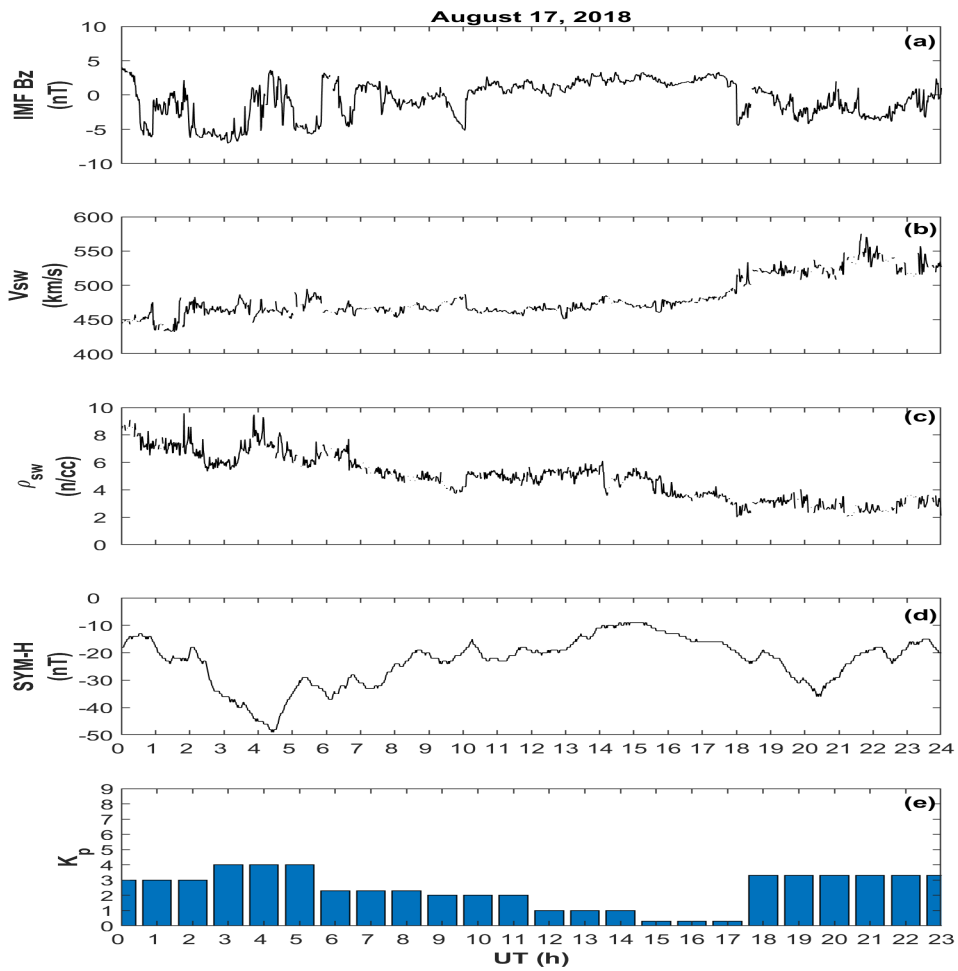


Figure 13: Variations of (a) IMF B_z (nT), (b) V_{sw} (km/s), (c) ρ_{sw} (n/cc), (d) SYM-H (nT) and (e) K_p during August 17, 2018.

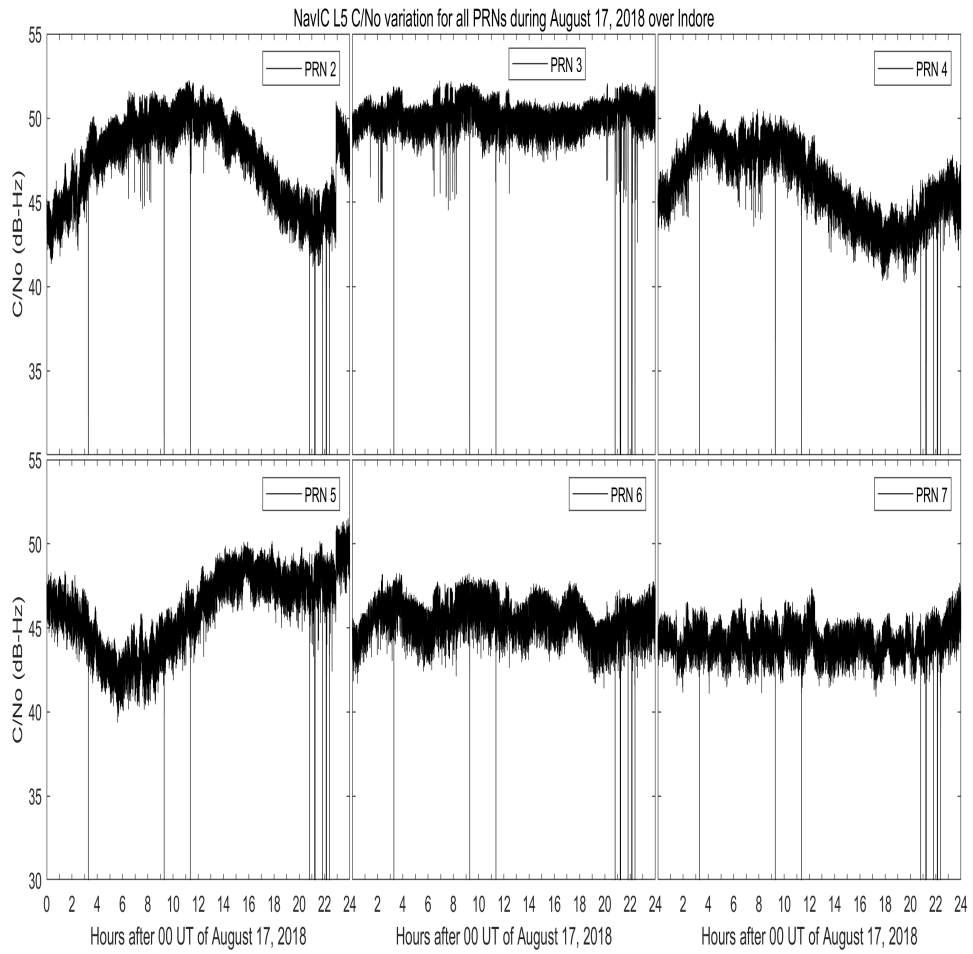


Figure 14: The C/N_o (dB-Hz) variation during the entire day of August 17, 2018, over Indore, as observed by the L5 signal of NavIC satellite PRNs 2-7.

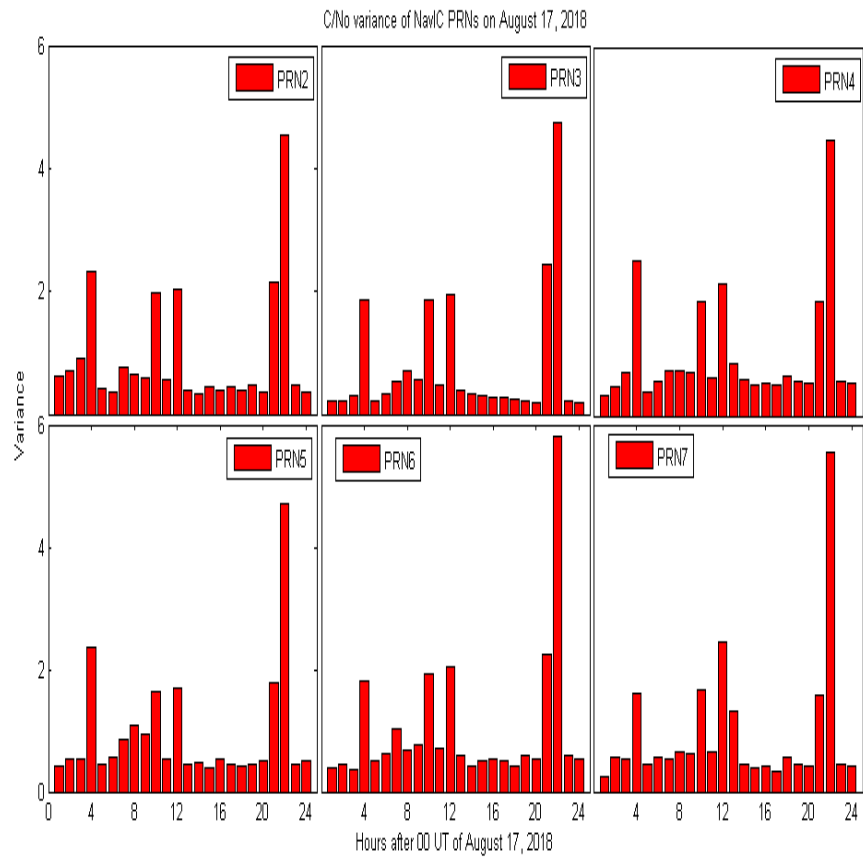


Figure 15: The hourly binned variance plots of C/N_o for all PRNs of NavIC on August 17, 2018, over Indore.

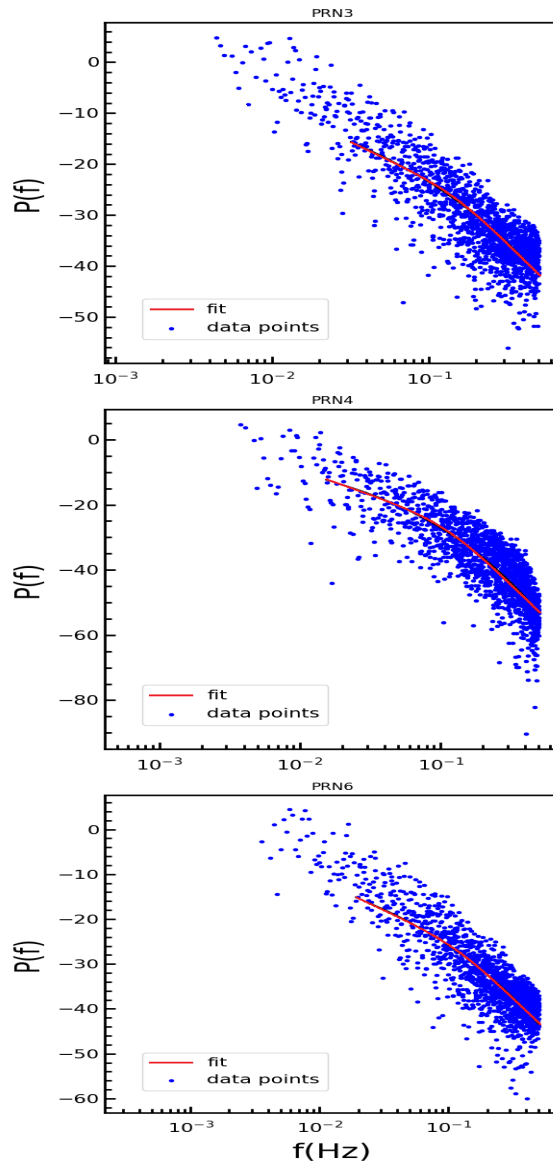


Figure 16: The PSD variations with the least square fit (red solid line) correspond to the time bins of C/N_o variation of Figure 15.

Finally, To understand the overall nature of the ionospheric variabilities as observed through NavIC and the corresponding irregularity scale sizes, during the entire analysis period from simultaneous observations over locations near the northern crest of EIA (Indore) and in between the crest and magnetic equator (Hyderabad), Table 1 summarizes the estimated values of the irregularity scale sizes, for all the 27 days consisting of events under strong, weak-to-moderate, and quiet geomagnetic storm intensities, all of which had occurred in different seasons over one year. The corresponding solar radio flux values (F10.7 in s.f.u) have also been presented in the same table to show the solar activity level during these days. The range of the outer scale sizes observed implies the presence of larger (order of a few km) and smaller (order of a few 100 m) scale structures over both locations. The overall variations show that the scale sizes during the stronger event had been around the order of a few km whereas, for the weak-to-moderate, and quiet-time conditions, they were of the order of a few hundred meters.

Table 1: The outer scale sizes of irregularities for all the 27 days of observation when the L5 C/N_o drops were observed under different geomagnetic conditions over the two locations: Indore (L_{Indr}) and Hyderabad (L_{Hyde}) are shown below. The 10.7 cm solar radio flux values (F10.7 in s.f.u) are indicated to show the corresponding solar activity level.

Cases	F10.7 (s.f.u)	Storm Intensity	L_{Indr} (km)	L_{Hyde} (km)
08/09/2017	188.5	strong	5.120 ± 0.011	5.150 ± 0.001
16/09/2017	72.9	moderate	0.507 ± 0.001	0.504 ± 0.086
27/09/2017	91.3	moderate	0.511 ± 0.010	0.499 ± 0.015
12/10/2017	69.9	moderate	0.517 ± 0.032	0.514 ± 0.021
24/10/2017	76.7	moderate	0.508 ± 0.007	0.506 ± 0.098
25/10/2017	77.9	moderate	0.480 ± 0.006	0.505 ± 0.093
01/12/2017	68.3	quiet	0.507 ± 0.005	0.512 ± 0.014
04/12/2017	66.4	weak	0.504 ± 0.085	0.489 ± 0.026
14/12/2017	69.8	quiet	0.506 ± 0.007	0.519 ± 0.039
27/12/2017	68.6	quiet	0.514 ± 0.015	0.502 ± 0.026
16/02/2018	69.8	quiet	0.524 ± 0.020	0.519 ± 0.021
19/02/2018	67.5	weak	0.521 ± 0.001	0.502 ± 0.056
20/02/2018	66.3	quiet	0.499 ± 0.048	0.498 ± 0.006
21/02/2018	68.7	quiet	0.511 ± 0.085	0.500 ± 0.018
22/02/2018	67.0	weak	0.514 ± 0.007	0.489 ± 0.085
24/02/2018	66.8	weak	0.490 ± 0.006	0.489 ± 0.026
25/02/2018	65.9	quiet	0.494 ± 0.090	0.481 ± 0.019
27/02/2018	66.6	moderate	0.512 ± 0.000	0.489 ± 0.099
28/02/2018	67.5	quiet	0.510 ± 0.097	0.489 ± 0.036
01/03/2018	66.0	quiet	0.495 ± 0.091	0.517 ± 0.030
02/03/2018	66.6	quiet	0.522 ± 0.005	0.509 ± 0.002
13/03/2018	67.7	quiet	0.507 ± 0.095	0.499 ± 0.015
22/03/2018	68.0	quiet	0.514 ± 0.001	0.519 ± 0.008
28/04/2018	71.1	quiet	0.486 ± 0.011	0.508 ± 0.054
28/05/2018	78.9	quiet	0.507 ± 0.009	0.502 ± 0.089
05/06/2018	73.4	quiet	0.517 ± 0.005	0.504 ± 0.001
17/08/2018	69.0	weak	0.502 ± 0.071	0.509 ± 0.092

4. Discussion

The low-latitude region over the globe is severely affected by the ionospheric scintillations, which degrades the performance of the satellite-based communication and navigational systems on which society is heavily dependent. The intermediate scale size irregularities (about a few 100 meters to a few km), which are the major sources of scintillations on the L-band and VHF transionospheric radio signals and scatter the high-frequency radio waves that are propagating through the low-to-equatorial ionosphere, are formed as a result of the R-T instability growth on the bottom side of the equatorial F-layer during the post-sunset local time. This scattering, in turn, creates a spatial pattern in the form of variations in the amplitude and phase of these signals on the receiver plane. Due to the relative movement of these irregularities with respect to the path of the signals that are transmitted from GNSS, the spatial patterns of amplitude and phase variations move past the receiver resulting in rapid temporal fluctuations in the phase and the amplitude of the signal that is being received by these ground-based GNSS receivers. On any given night, these intermediate-scale size irregularities associated with the EPBs can cover a large portion of the ionosphere over a particular longitude sector in the low-latitude regions (Bhattacharyya (2019) and references therein).

It is well known that the F-region ionospheric irregularities exhibit power law spectra. For various conditions of the ionosphere, the power law dependence is universal and has been verified by various researchers (Rufenach (1972); Singleton (1974); Crane (1976); Umeki et al. (1977); Franke and Liu (1983) and references therein) using multiple measurements. A power law

variation would signify the existence of some non-linear processes. These cascade-type processes would allow energy (the wind shears or solar heating) inflow to get redistributed across the various scales in addition to the larger inhomogeneities (energy-containing inhomogeneities of the largest size called the outer scale) getting split (due to the bending and stretching under the inertial forces) into the less energetic and smaller inhomogeneities. This process continues till the smallest inhomogeneity scale (inner scale) is reached, where the viscous forces dominate the inertial forces and the dissipation of energy takes place (Vasylyev et al., 2022).

In the phase screen model (Rino, 1979a,b) given by Rino, the spectral slopes obtained from the PSD analysis are considered as a key parameter for the accurate determination of the level or intensity of scintillation (Aol et al., 2023). Looking back at the case studies in the present investigation, we observe that for the September 08, 2017 event, the values of the spectral slopes were around -3.6. This is close to the value of $-11/3$. The ionospheric structures that were present during that particular day produced a power law spectral nature closely resembling the Kolmogorov ($-5/3$) spectrum, the slope ($-11/3$) being the characteristic feature of that turbulence. This type of spectral slope gets generated by the injection of energy (geomagnetic field disturbances, instabilities due to solar forcing, etc.) into the system at large scales and the non-linear transfer of energy from the larger structures to the smaller ones, via the evolution of turbulence through the non-linear interactions between the fluctuations in plasma. Here the $-11/3$ slope suggests the process of anisotropic cascading of turbulent energy. This energy eventually dissipates, at smaller scales, via the mechanism of wave-particle interactions

and/or ion-neutral collisions (Clifford (1978); Kelley and Ott (1978); Lane et al. (1992); Davidson (2015); Guio and Pecseli (2021); Vasylyev et al. (2022) and references therein). For the cases of September 16, 2017, and August 17, 2018, the spectral slopes were around -2.8 and -2.5 respectively, which is close to the value of $-8/3$. This type of spectral slope is observed in regions where small-scale irregularities are dominant as a result of instabilities (strongly anisotropic and intermittent turbulence) at these scales and suggest rapid/steeper decay of energy compared to a Kolmogorov turbulent cascade, at these smaller scales.

Furthermore, Figure 17 shows the C/N_o variations of NavIC PRNs 5 and 6 in red as observed over Indore and in blue as observed over Hyderabad for the respective bins when there are significant drops as observed from the variance plots (i.e. Figure 4). Now, as the F-region ionospheric irregularities over the geomagnetic equator get mapped along the geomagnetic field lines to latitudes away from the equator (near and around the crest regions), a time delay in scintillation occurrence, as a result of the movement of these irregularity structures, is expected when observing over a region (Indore) close to the crest in comparison to a region (Hyderabad) away from the crest. In Figure 17, the C/N_o drops observed by PRNs 5 and 6 are at 18:25 UT (23:29 LT) and 17:06 UT (22:10 LT) respectively over Indore and the same at 17:49 UT (23:03 LT) and 16:16 UT (21:30 LT) over Hyderabad, suggesting a clear time delay, of scintillation occurrence and a poleward movement of the plasma irregularity structures, for about 36 minutes for PRN 5 and 50 minutes for PRN 6 over Indore with respect to that over Hyderabad.

Next, the geographic locations of IPPs for PRNs 5 and 6 are (21.13°N ,

79.42°E) and (21.58°N, 71.28°E) respectively over Indore, and (16.55°N, 82.65°E) and (16.26°N, 74.45°E) respectively over Hyderabad. Interestingly, on observing the time of C/N_o drops over the two locations and the two PRNs in Figure 17 along with the comparison with the longitudes of the PRN IPPs over these two locations, we can observe a westward propagation of the large-scale (km) plasma irregularity structures over these regions. As the IPPs of the two PRNs over Hyderabad are eastward in comparison to the same over Indore, and we observe scintillation over Hyderabad first, it is clear that the irregularity structures drifted westward. It is to be noted that the observed westward propagation of the irregularity structures in the present study is consistent with the study presented in (Li et al., 2018) when an under-shielding condition of penetration electric field was present over these locations of observations and could have been a factor to have caused such westward drift of the irregularity structures.

An important proxy for scintillation occurrence and identification of the associated ionospheric disturbances and irregularity structures is the Rate of TEC Index (ROTI). This is the standard deviation of the Rate of change of TEC (ROT) over 5 minutes (Pi et al. (1997); Tiwari et al. (2013) and references therein). Further, if this ROTI shows values above 0.5 TECU/min, it would indicate the presence of a few km order of irregularity scale sizes (Ma and Maruyama, 2006). Following these studies and to validate the presence of km scale sizes of irregularities on September 08, 2017, over the Indian sector, we show the variation of ROTI in Figure 18. The time duration is taken from 16:00 to 20:00 UT keeping in mind the occurrences of scintillations, shown earlier, between these periods on this day. These ROTI values

are calculated from the GNSS/GPS data available at the IGS stations: Lucknow (26.91°N, 80.96°E, dip: 39.75°N) and Kanpur (26.52°N, 80.23°E, dip: 38.52°N) located beyond the EIA crest, and Hyderabad (17.42°N, 78.55°E, dip: 21.69°N) and Bengaluru (13.02°N, 77.57°E, dip: 11.71°N) located away from the crest and closest to dip equator respectively. The Indore (22.52°N, 75.92°E, dip: 32.23°N and located near the EIA crest) data is obtained from the GNSS/GPS receiver available at IIT Indore. From this figure, there are multiple instances of ROTI values greater than 0.5 TECU/min, suggesting the presence of irregularities of the order of a few km that caused scintillations in the L-band signals of these satellites. It is to be noted that upon similar analysis (not shown) of the ROTI from these stations for the other events, we could observe the ROTI values to be well below 0.5 TECU/min, suggesting much smaller (few 100 m) irregularity scale sizes were present.

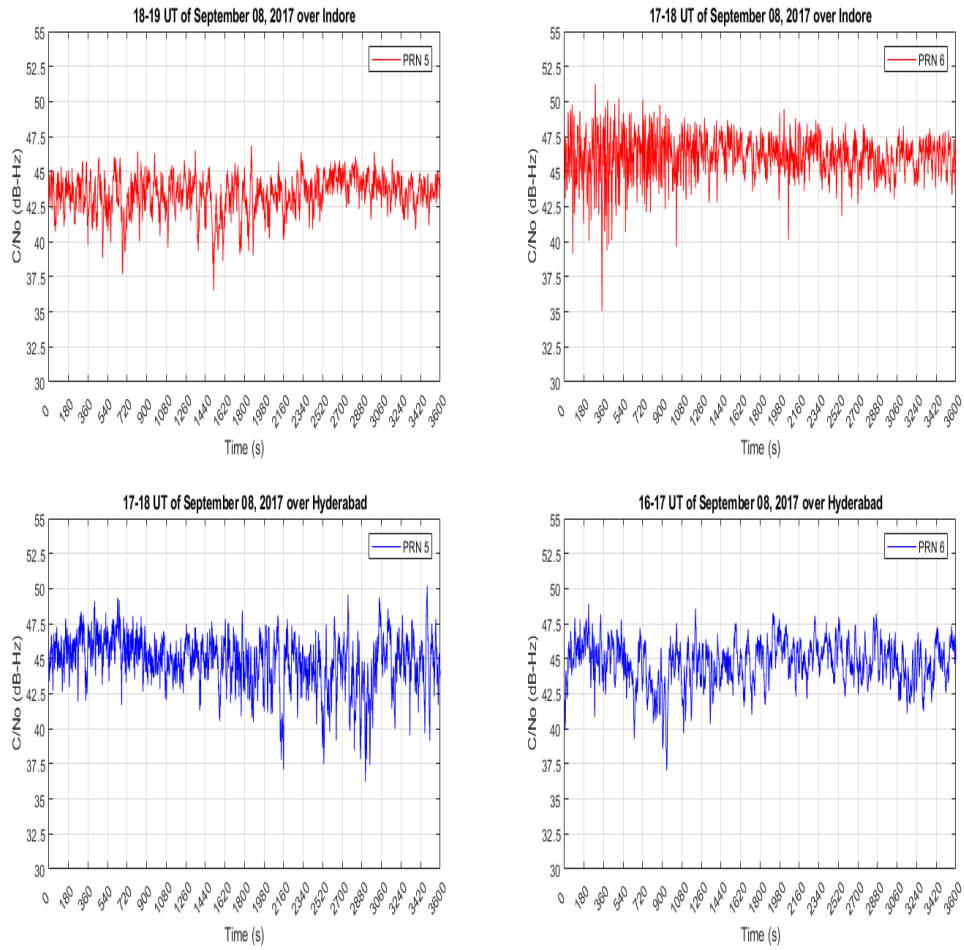


Figure 17: The C/N_o (dB-Hz) variation during significant time bins of September 08, 2017, as observed by the L5 signal of NavIC satellite PRNs 5 and 6 over both Indore and Hyderabad. For Indore, LT (h) = $UT + 05:04$ and for Hyderabad, LT (h) = $UT + 05:14$

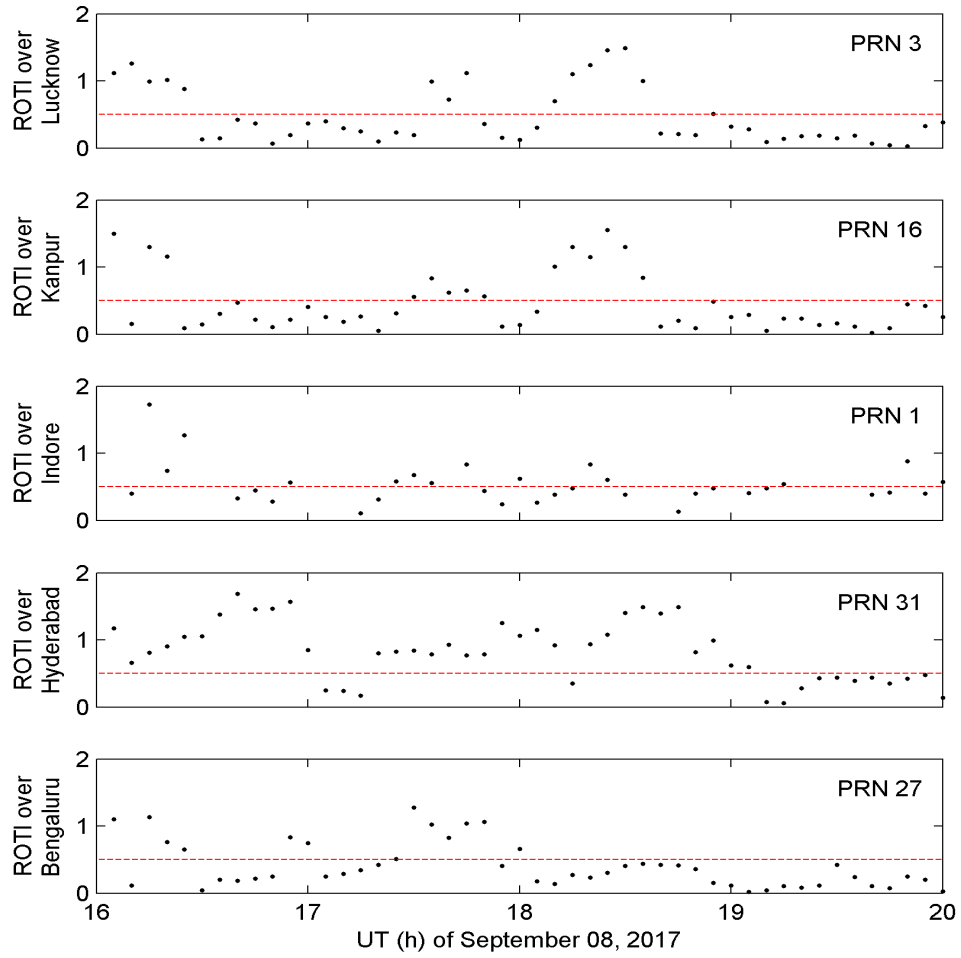


Figure 18: The GNSS/GPS ROTI (TECU/min) variation along with the satellite PRNs during September 08, 2017. From top to bottom: The stations (Lucknow to Bengaluru) are arranged as one goes from beyond the EIA crest towards the dip equator. The values of 0.5 TECU/min have been indicated by red-dashed horizontal lines.

5. Summary

The ionosphere over the Indian longitude sector is highly dynamic and geosensitive due to the presence of the northern crest of EIA and the magnetic equator. A study of the ionospheric irregularities, that have drastic impacts on the performance of the global navigational satellite systems in and around these locations under geomagnetically active conditions, is essential. The detailed study of these ionospheric irregularities brings forward important aspects to understanding ionospheric physics and related processes. To address this issue, the present work investigated the simultaneous observations of low-latitude ionospheric irregularities over locations chosen to cover the zones of both the northern crest of EIA (Indore) and in between the crest and the magnetic equator (Hyderabad). This study utilized the L5 signal C/N_o variations from a set of GEO and GSO satellites of NavIC for determining the irregularity spectral slope and the corresponding outer irregularity scale sizes, using the PSD analysis. The estimated scale sizes ranged from about 500 m over Indore and Hyderabad under weak-to-moderate and quiet-time conditions and about 5 km over both locations under the strong geomagnetic event. These scale sizes were further validated by the ROTI variations. Further, a time delay of scintillation occurrence over Indore, with values of 36 minutes and 50 minutes for NavIC PRNs 5 and 6 respectively, from scintillation occurrence at Hyderabad, was also observed. This observation suggested a poleward evolution of the irregularity structures on the event day. Furthermore, a westward propagation of these km-scale irregularity structures, was observed. This observation is consistent with the observations shown in the work by (Li et al., 2018). Therefore, this study brought forward the useful-

ness of monitoring the propagation and evolution of low-latitude ionospheric irregularities with simultaneous observations, from a region near the crest and another away from it, utilizing observations from a continuously available set of GEO and GSO navigation satellite systems.

Acknowledgments

SC acknowledges the Space Applications Centre (SAC), ISRO for providing a research fellowship under the project NGP-17 during his doctoral tenure. The authors acknowledge SAC/ISRO for providing the NavIC receivers to the Department of Astronomy, Astrophysics and Space Engineering (DAASE), IIT Indore under this project. AD acknowledges the use of facilities procured through the funding via the Department of Science and Technology (DST), Government of India (GoI) sponsored DST-FIST grant no. SR/FST/PSII/2021/162 (C) awarded to the DAASE, IIT Indore. The authors also acknowledge the Department of ECE, Osmania University for providing us with the NavIC data of Hyderabad. The authors also acknowledge Prof. Gopi K. Seemala of the Indian Institute of Geomagnetism (IIG), Navi Mumbai, India for providing the software available from <https://seemala.blogspot.com/2017/09/gps-tec-program-ver-295.html?m=1> to analyze the IGS data available at <http://sopac-csrc.ucsd.edu/index.php/data-download/>. The authors acknowledge the valuable comments and suggestions from all the reviewers that have significantly enriched the manuscript's quality. SC also acknowledges Aishrila Mazumder for fruitful discussions. Further acknowledgments go to the World Data Center for Geomagnetism, Kyoto at <https://wdc.kugi.kyoto-u.ac.jp/kp/index.html> for the K_p index and

the SPDF OMNIWeb database at <https://omniweb.gsfc.nasa.gov/>, for the high-resolution (1-minute) IMF B_z , V_{sw} , ρ_{sw} , and the SYM-H data.

References

- Aol, S., Buchert, S., Jurua, E., 2020. Ionospheric irregularities and scintillations: a direct comparison of in situ density observations with ground-based l-band receivers. *Earth, Planets and Space* 72, 164. URL: <https://doi.org/10.1186/s40623-020-01294-z>.
- Aol, S., Buchert, S., Jurua, E., Sorriso-Valvo, L., 2023. Spectral properties of sub-kilometer-scale equatorial irregularities as seen by the swarm satellites. *Advances in Space Research* 72, 741–752. URL: <https://www.sciencedirect.com/science/article/pii/S0273117722006895>. space and Geophysical Observations and Recent Results related to the African Continent.
- Ayyagari, D., Chakraborty, S., Das, S., Shukla, A., Paul, A., Datta, A., 2020. Performance of navic for studying the ionosphere at an eia region in india. *Advances in Space Research* 65, 1544 – 1558. URL: <https://doi.org/10.1016/j.asr.2019.12.019>.
- Ayyagari, D., Chakraborty, S., Datta, A., 2019. Ionospheric observations over central part of india using comparative study of navic and gnss, in: 2019 URSI Asia-Pacific Radio Science Conference (AP-RASC), pp. 1–2. URL: <https://doi.org/10.23919/URSIAP-RASC.2019.8738244>.
- Ayyagari, D., Chakraborty, S., Datta, A., 2020. A short note on estimates of position coordinates of NavIC during an intense geomagnetic storm day at

- Indore., in: AGU Fall Meeting Abstracts, pp. SM003–0008. URL: <https://ui.adsabs.harvard.edu/abs/2020AGUFMSM0030008A/abstract>.
- Ayyagari, D., Chakraborty, S., Datta, A., Das, S., 2021. Impact of intense geomagnetic storm on navic signals over indore, in: Das, N.R., Sarkar, S. (Eds.), *Computers and Devices for Communication*, Springer Singapore, Singapore. pp. 157–162. URL: https://doi.org/10.1007/978-981-15-8366-7_21.
- Ayyagari, D., Datta, A., Chakraborty, S., 2022. Systematic study of ionospheric scintillation over the indian low-latitudes during low solar activity conditions. *Advances in Space Research* 70, 2506–2521. URL: <https://www.sciencedirect.com/science/article/pii/S0273117722006275>.
- Basu, S., Basu, S., Weber, E.J., Coley, W.R., 1988a. Case study of polar cap scintillation modeling using de 2 irregularity measurements at 800 km. *Radio Science* 23, 545–553. URL: <https://agupubs.onlinelibrary.wiley.com/doi/abs/10.1029/RS023i004p00545>.
- Basu, S., MacKenzie, E., Basu, S., 1988b. Ionospheric constraints on vhf/uhf communications links during solar maximum and minimum periods. *Radio Science* 23, 363–378. URL: <https://agupubs.onlinelibrary.wiley.com/doi/abs/10.1029/RS023i003p00363>.
- Bhattacharyya, A., 1999. Deterministic retrieval of ionospheric phase screen from amplitude scintillations. *Radio Science* 34, 229–240. URL: <https://agupubs.onlinelibrary.wiley.com/doi/abs/10.1029/98RS02351>.

- Bhattacharyya, A., 2019. Challenges of predicting low-latitude ionospheric scintillations. *URSI Radio Science Bulletin* 2019, 17–31. URL: <https://doi.org/10.23919/URSIRSB.2019.9117241>.
- Bhattacharyya, A., Beach, T.L., Basu, S., Kintner, P.M., 2000. Night-time equatorial ionosphere: Gps scintillations and differential carrier phase fluctuations. *Radio Science* 35, 209–224. URL: <https://agupubs.onlinelibrary.wiley.com/doi/abs/10.1029/1999RS002213>.
- Booker, H.G., Ratcliffe, J.A., Shinn, D.H., Bragg, W.L., 1950. Diffraction from an irregular screen with applications to ionospheric problems. *Philosophical Transactions of the Royal Society of London. Series A, Mathematical and Physical Sciences* 242, 579–607. URL: <https://royalsocietypublishing.org/doi/abs/10.1098/rsta.1950.0011>.
- Carrano, C.S., Groves, K.M., Caton, R.G., 2012a. The effect of phase scintillations on the accuracy of phase screen simulation using deterministic screens derived from gps and altair measurements. *Radio Science* 47. URL: <https://agupubs.onlinelibrary.wiley.com/doi/abs/10.1029/2011RS004958>.
- Carrano, C.S., Groves, K.M., Caton, R.G., Rino, C.L., Straus, P.R., 2011. Multiple phase screen modeling of ionospheric scintillation along radio occultation raypaths. *Radio Science* 46. URL: <https://agupubs.onlinelibrary.wiley.com/doi/abs/10.1029/2010RS004591>.
- Carrano, C.S., Rino, C.L., 2016. A theory of scintillation for two-component power law irregularity spectra: Overview and numerical results. *Radio Sci-*

- ence 51, 789–813. URL: <https://agupubs.onlinelibrary.wiley.com/doi/abs/10.1002/2015RS005903>.
- Carrano, C.S., Valladares, C.E., Groves, K.M., 2012b. Latitudinal and local time variation of ionospheric turbulence parameters during the conjugate point equatorial experiment in brazil. *International Journal of Geophysics* 2012, 103963. URL: <https://doi.org/10.1155/2012/103963>.
- Caton, R.G., Carrano, C.S., Alcala, C.M., Groves, K.M., Beach, T., Sponseller, D., 2009. Simulating the effects of scintillation on transionospheric signals with a two-way phase screen constructed from altair phase-derived tec. *Radio Science* 44. URL: <https://agupubs.onlinelibrary.wiley.com/doi/abs/10.1029/2008RS004047>.
- Chakraborty, S., 2022. Evidence of changes in the low-latitude plasma drift under imf bz coupling: a tiegcm simulation approach, in: 2022 3rd URSI Atlantic and Asia Pacific Radio Science Meeting (AT-AP-RASC), pp. 1–4. URL: <https://doi.org/10.23919/AT-AP-RASC54737.2022.9814304>.
- Chakraborty, S., Chakrabarty, D., 2023. Global asymmetry in Δx variations during the 06 april 2000 geomagnetic storm: Relative roles of imf bz and by. *Journal of Geophysical Research: Space Physics* 128, e2022JA031047. URL: <https://agupubs.onlinelibrary.wiley.com/doi/abs/10.1029/2022JA031047>.
- Chakraborty, S., Datta, A., 2020a. Assessment of the performance of ionospheric models with navic observations during geomagnetic storms, in:

- 2020 URSI Regional Conference on Radio Science (URSI-RCRS), pp. 1–4. URL: <https://doi.org/10.23919/URSIRCRS49211.2020.9113547>.
- Chakraborty, S., Datta, A., 2020b. Impact of Solar Activity on the Magnetosphere-Ionosphere-Thermosphere system over the geophysically sensitive Indian subcontinent. *Bulletin of the AAS* 52. URL: <https://baas.aas.org/pub/aas236-112p01-chakraborty/release/1>.
- Chakraborty, S., Datta, A., 2020c. Geomagnetic Storm-time Ionospheric Response over Locations around the EIA and the Magnetic Equator, in: *AGU Fall Meeting Abstracts*, pp. SA021–0020. URL: <https://ui.adsabs.harvard.edu/abs/2020AGUFMSA0210020C/abstract>.
- Chakraborty, S., Datta, A., 2021. Study of low-latitude ionospheric scintillation using navic, in: *2021 XXXIVth General Assembly and Scientific Symposium of the International Union of Radio Science (URSI GASS)*, pp. 1–3. URL: <https://doi.org/10.23919/URSIGASS51995.2021.9560192>.
- Chakraborty, S., Datta, A., Ray, S., Ayyagari, D., Paul, A., 2020b. Comparative studies of ionospheric models with gnss and navic over the indian longitudinal sector during geomagnetic activities. *Advances in Space Research* 66, 895 – 910. URL: <http://www.sciencedirect.com/science/article/pii/S0273117720302994>.
- Chakraborty, S., Ray, S., Datta, A., Paul, A., 2020. Ionospheric response to strong geomagnetic storms during 2000–2005: An imf clock angle perspective. *Radio Science* 55, e2020RS007061. URL: <https://agupubs.onlinelibrary.wiley.com/doi/abs/10.1029/2020RS007061>.

- Chakraborty, S., Ray, S., Sur, D., Datta, A., Paul, A., 2020a. Effects of cme and cir induced geomagnetic storms on low-latitude ionization over indian longitudes in terms of neutral dynamics. *Advances in Space Research* 65, 198 – 213. URL: <http://www.sciencedirect.com/science/article/pii/S0273117719307252>.
- Clifford, S.F., 1978. The classical theory of wave propagation in a turbulent medium. Springer Berlin Heidelberg, Berlin, Heidelberg. chapter 16. pp. 9–43. URL: [https://doi.org/10.1007/3540088121\\$_16](https://doi.org/10.1007/3540088121$_16).
- Costa, E., de Paula, E.R., Rezende, L.F.C., Groves, K.M., Roddy, P.A., Dao, E.V., Kelley, M.C., 2011. Equatorial scintillation calculations based on coherent scatter radar and c/nofs data. *Radio Science* 46. URL: <https://agupubs.onlinelibrary.wiley.com/doi/abs/10.1029/2010RS004435>.
- Crane, R.K., 1976. Spectra of ionospheric scintillation. *Journal of Geophysical Research* (1896-1977) 81, 2041–2050. URL: <https://agupubs.onlinelibrary.wiley.com/doi/abs/10.1029/JA081i013p02041>.
- Davidson, P., 2015. *Turbulence: An Introduction for Scientists and Engineers*. Oxford University Press. URL: <https://doi.org/10.1093/acprof:oso/9780198722588.001.0001>.
- Fougere, P.F., 1985. On the accuracy of spectrum analysis of red noise processes using maximum entropy and periodogram methods: Simulation studies and application to geophysical data. *Journal of Geophysical Research: Space Physics* 90, 4355–4366. URL: <https://agupubs.onlinelibrary.wiley.com/doi/abs/10.1029/JA090iA05p04355>.

- Franke, S.J., Liu, C.H., 1983. Observations and modeling of multi-frequency vhf and ghz scintillations in the equatorial region. *Journal of Geophysical Research: Space Physics* 88, 7075–7085. URL: <https://agupubs.onlinelibrary.wiley.com/doi/abs/10.1029/JA088iA09p07075>.
- Guio, P., Pecseli, H.L., 2021. The impact of turbulence on the ionosphere and magnetosphere. *Frontiers in Astronomy and Space Sciences* 7. URL: <https://www.frontiersin.org/journals/astronomy-and-space-sciences/articles/10.3389/fspas.2020.573746>.
- Hewish, A., Bragg, W.L., 1951. The diffraction of radio waves in passing through a phase-changing ionosphere. *Proceedings of the Royal Society of London. Series A. Mathematical and Physical Sciences* 209, 81–96. URL: <https://royalsocietypublishing.org/doi/abs/10.1098/rspa.1951.0189>.
- Kelley, M.C., Ott, E., 1978. Two-dimensional turbulence in equatorial spread f. *Journal of Geophysical Research: Space Physics* 83, 4369–4372. URL: <https://doi.org/10.1029/JA083iA09p04369>.
- Knepp, D.L., 2004. Effects of ionospheric scintillation on transit satellite measurement of total electron content. *Radio Science* 39. URL: <https://agupubs.onlinelibrary.wiley.com/doi/abs/10.1029/2002RS002825>.
- Knepp, D.L., Nickisch, L.J., 2009. Multiple phase screen calculation of wide bandwidth propagation. *Radio Science* 44. URL: <https://agupubs.onlinelibrary.wiley.com/doi/abs/10.1029/2008RS004054>.

- Lane, R.G., Glindemann, A., Dainty, J.C., 1992. Simulation of a kolmogorov phase screen. *Waves in Random Media* 2, 209–224. URL: <https://doi.org/10.1088/0959-7174/2/3/003>.
- Li, G., Ning, B., Wang, C., Abdu, M.A., Otsuka, Y., Yamamoto, M., Wu, J., Chen, J., 2018. Storm-enhanced development of postsunset equatorial plasma bubbles around the meridian 120°e/60°w on 7–8 september 2017. *Journal of Geophysical Research: Space Physics* 123, 7985–7998. URL: <https://agupubs.onlinelibrary.wiley.com/doi/abs/10.1029/2018JA025871>.
- Liu, Y.H., Liu, C.H., Su, S.Y., 2012. Global and seasonal scintillation morphology in the equatorial region derived from ROCSAT-1 in-situ data. *Terr. Atmos. Ocean. Sci.* 23, 95–106. URL: [https://doi.org/10.3319/TAO.2011.06.30.01\(AA\)](https://doi.org/10.3319/TAO.2011.06.30.01(AA)).
- Loewe, C.A., Probst, G.W., 1997. Classification and mean behavior of magnetic storms. *Journal of Geophysical Research: Space Physics* 102, 14209–14213. URL: <https://doi.org/10.1029/96JA04020>.
- Ma, G., Maruyama, T., 2006. A super bubble detected by dense gps network at east asian longitudes. *Geophysical Research Letters* 33. URL: <https://agupubs.onlinelibrary.wiley.com/doi/abs/10.1029/2006GL027512>.
- de Oliveira Moraes, A., Costa, E., Abdu, M.A., Rodrigues, F.S., de Paula, E.R., Oliveira, K., Perrella, W.J., 2017. The variability of low-latitude ionospheric amplitude and phase scintillation detected by a triple-

- frequency gps receiver. *Radio Science* 52, 439–460. URL: <https://agupubs.onlinelibrary.wiley.com/doi/abs/10.1002/2016RS006165>.
- Pi, X., Mannucci, A.J., Lindqwister, U.J., Ho, C.M., 1997. Monitoring of global ionospheric irregularities using the worldwide gps network. *Geophysical Research Letters* 24, 2283–2286. URL: <https://agupubs.onlinelibrary.wiley.com/doi/abs/10.1029/97GL02273>.
- Priyadarshi, S., 2015. A review of ionospheric scintillation models. *Surveys in Geophysics* 36, 295–324. URL: <https://doi.org/10.1007/s10712-015-9319-1>.
- Rino, C.L., 1979a. A power law phase screen model for ionospheric scintillation: 1. weak scatter. *Radio Science* 14, 1135–1145. URL: <https://agupubs.onlinelibrary.wiley.com/doi/abs/10.1029/RS014i006p01135>.
- Rino, C.L., 1979b. A power law phase screen model for ionospheric scintillation: 2. strong scatter. *Radio Science* 14, 1147–1155. URL: <https://agupubs.onlinelibrary.wiley.com/doi/abs/10.1029/RS014i006p01147>.
- Rufenach, C.L., 1972. Power-law wavenumber spectrum deduced from ionospheric scintillation observations. *Journal of Geophysical Research (1896-1977)* 77, 4761–4772. URL: <https://agupubs.onlinelibrary.wiley.com/doi/abs/10.1029/JA077i025p04761>.
- Secan, J.A., Bussey, R.M., Fremouw, E.J., Basu, S., 1995. An improved

- model of equatorial scintillation. *Radio Science* 30, 607–617. URL: <https://agupubs.onlinelibrary.wiley.com/doi/abs/10.1029/94RS03172>.
- Singleton, D., 1974. Power spectra of ionospheric scintillations. *Journal of Atmospheric and Terrestrial Physics* 36, 113–133. URL: <https://www.sciencedirect.com/science/article/pii/0021916974900713>.
- Strangeways, H.J., 2009. Determining scintillation effects on gps receivers. *Radio Science* 44. URL: <https://agupubs.onlinelibrary.wiley.com/doi/abs/10.1029/2008RS004076>.
- Taylor, L.S., Infosino, C.J., 1976. On the strong phase screen theory of ionospheric scintillations. *Radio Science* 11, 459–463. URL: <https://agupubs.onlinelibrary.wiley.com/doi/abs/10.1029/RS011i005p00459>.
- Tiwari, R., Strangeways, H., Tiwari, S., Ahmed, A., 2013. Investigation of ionospheric irregularities and scintillation using tec at high latitude. *Advances in Space Research* 52, 1111–1124. URL: <https://www.sciencedirect.com/science/article/pii/S0273117713003517>.
- Umeki, R., Liu, C.H., Yeh, K.C., 1977. Multifrequency spectra of ionospheric amplitude scintillations. *Journal of Geophysical Research (1896-1977)* 82, 2752–2760. URL: <https://agupubs.onlinelibrary.wiley.com/doi/abs/10.1029/JA082i019p02752>.
- Vasylyev, D., Bacniguel, Y., Volker, W., Kriegel, M., Berdermann, J., 2022. Modeling of ionospheric scintillation. *J. Space Weather Space Clim.* 12, 22. URL: <https://doi.org/10.1051/swsc/2022016>.

Yeh, K.C., Liu, C.H., 1982. Radio wave scintillations in the ionosphere.
Proceedings of the IEEE 70, 324–360. URL: [https://doi.org/10.1109/
PROC.1982.12313](https://doi.org/10.1109/PROC.1982.12313).